Planetary and Space Science 276–277 (2026) 106292

Contents lists available at ScienceDirect

Planetary and Space Science

journal homepage: www.elsevier.com/locate/pss

# Simulating planetary surface reactions with an environmentally controlled experiment chamber

Chengzheng Yong *, Alian Wang, Chuck Y.C. Yan, Bradley L. Jolliff

*Department of Earth, Environmental, and Planetary Sciences and the McDonnell Center for the Space Sciences, Washington University in St. Louis, St. Louis, MO, 63130, USA*

ARTICLE INFO

*Keywords:*
Planetary simulation chamber
Raman spectroscopy
Plasma spectroscopy
Performance tests
Applications

ABSTRACT

Because of significant challenges posed by space exploration missions, experiments in simulation chambers could shed light on certain planetary processes of interest to support mission design and mission data interpretation, as well as for testing science payloads for missions. Here we present our planetary environment simulation system built at Washington University in St. Louis. The system includes a two-layer vacuum baking chamber for sample preparation and a vacuum reaction chamber (upgraded planetary environment and analysis chamber, PEACh) featuring controllable temperature, pressure, and gas composition. The upgraded PEACh can simulate water-rock interaction via a water injection port, and it can simulate space weathering by using an energetic electron impact (EEI) accessory. In addition, this vacuum reaction chamber is equipped with in-situ monitoring probes, including Raman spectroscopy and plasma spectroscopy, as well as a video camera. The whole system is mainly designed for simulating water-regolith interactions in the lunar polar regions, but it can also simulate other planetary environments, such as conditions at the Martian surface.

## 1. Introduction

Over the past two decades, and still today, much of the interest in planetary research has focused on the Moon, partly because $H_2O$/OH, together with other volatile substances, has been discovered in the polar regions of the Moon, such as Lunar Prospector (Feldman et al., 2000), Cassini (Clark, 2009), Deep Impact (Sunshine et al., 2009), Chandrayaan-1 (Pieters et al., 2009), LCROSS (Colaprete et al., 2010), and the Lunar Reconnaissance Orbiter (Campbell, 2016; Sanin et al., 2012). Specifically, determining the molecular forms and concentrations of the volatiles have become key objectives of many lunar exploration missions in the near future. The storage form of water on the Moon is still unknown owing to the lack of sampling and in-situ measurements. However, based on our understanding of lunar surface temperatures, the water-rock interactions that occur on other planets, and the discoveries of secondary minerals in asteroids (Perronnet et al., 2007; Suttle et al., 2022), we can infer the presence of secondary minerals in polar regions of the Moon (Stopar et al., 2018), where missions have not yet successfully landed. Through the simulation of water-regolith reactions in the lunar circumpolar regions, we are able to support spectral libraries, potential reaction pathways, and possible locations (including depth) of secondary minerals for the near-future lunar missions, including VIPER (Colaprete et al., 2019), Artemis 3 (R. C. Weber et al., 2021), and Chang'E 7 (C. Wang et al., 2024). Such research would be helpful in planning in-situ resource utilization (ISRU) and selecting sites for future lunar bases or science research stations. The same logic could be applied to other planetary bodies as well, including Mars and icy moons for astrobiology studies, i.e., simulating certain chemical reactions in a simulated martian or icy moon environment.

The remote sensing techniques of visible to near-infrared spectroscopy have been used to investigate the Moon via LRO, Chandrayaan, Kaguya, and Chang'E missions. However, these techniques are difficult to use in the polar regions, especially the permanently shaded regions (PSRs) and shallow subsurface owing to unfavorable illumination conditions. More direct means of volatile detection were used by neutron spectrometers (Feldman et al., 1998, 2000) and by the LCROSS mission, which impacted a PSR and analyzed volatile species directly in the plume created by the impact (Colaprete et al., 2010).

The focus of lunar missions in the near future is to land in the polar regions to explore areas of potential volatile deposits in-situ. Laboratory

This article is part of a special issue entitled: Planetary Simulants published in Planetary and Space Science.

* Corresponding author.
*E-mail address:* chengzheng@wustl.edu (C. Yong).

https://doi.org/10.1016/j.pss.2026.106292
Received 19 December 2025; Received in revised form 29 April 2026; Accepted 8 May 2026
Available online 11 May 2026

characterization methods can be used to prepare for such exploration. For example, we can test Raman spectroscopy on secondary minerals produced by water-regolith reactions. Raman spectroscopy has not been applied in lunar missions because it must be done in-situ, on the lunar surface (A. Wang et al., 1998). For a lander or rover mission, Raman spectroscopy has some advantages compared to IR spectroscopy. First, the Raman peaks of a mineral, when present, are simple and narrow, and usually not overlapped with the peaks of other minerals. Second, there is no complicated calibration, thermal correction, or radiative transfer modeling needed for processing Raman data, hence reducing errors and ambiguities in data processing. Third, some molecular vibration modes only occur in Raman spectra (i.e., those from double-atom molecules) (Schrader, 1995; A. Wang et al., 1995). If we can integrate both Raman and IR spectroscopy, we could investigate planetary materials more comprehensively. Raman spectrometers are already used in missions to Mars (Beegle et al., 2015; Maurice et al., 2021), and planned in lunar missions, including the lunar Raman spectrometer (LRS) on the Chang'E 7 rover (C. Wang et al., 2024), the Raman Laser Spectrometer (RLS) on the ExoMars Rosalind Franklin Mission (Veneranda et al., 2020), and the Raman spectrometer for MMX (RAX) in the Martian Moons eXploration mission (Cho et al., 2021).

Many laboratories around the world have planetary simulation chambers, each with distinctive capabilities (Buffo et al., 2025; Craig et al., 2001; Donaldson Hanna et al., 2021; Gillis, 2022; Herczku et al., 2021; Herny et al., 2019; Mateo-Martí et al., 2006; Mattioda et al., 2024; Palumbo et al., 2004; Rabbow et al., 2016; Sears et al., 2002; Vakkada Ramachandran et al., 2020; I. Weber et al., 2022, 2024; Wu et al., 2021). These chambers can simulate a wide range of environments and planetary processes, including space weathering, UV radiation, ultra-high pressure, cryogenic ice deposition, and some have in-situ IR spectrometers or Raman spectrometers. However, our chamber uniquely combines a vacuum chamber with an in-situ Raman probe, an electron impact device, and a liquid water injection function. Together these attributes can advance the in-situ Raman study of hydration and dehydration cycles in lunar polar regions, especially in the subsurface.

The Planetary Environment and Analysis Chamber (PEACh) at Washington University in St. Louis (WashU) was originally built for Mars environment simulations (Sobron and Wang, 2012). The main functions include controlling the pressure, temperature, and gas composition, and applying many sensors inside the chamber including a laser Raman Probe, LIBS (Laser Induced Breakdown Spectroscopy), IR (infrared) and a microscopic imager. The PEACh can provide in-situ measurement of various spectra in a simulated martian environment. The initial aim was to establish a spectral library to aid the interpretation of data from Mars missions (MER, MSL, Mars Express, MRO, and ExoMars), by measuring a variety of spectra of relevant minerals inside the PEACh under different environmental parameters (temperature, RH, or gas composition).

Noting the new wave of lunar exploration and the expansion of Commercial Lunar Payload Services (CLPS) missions, we modified the PEACh to make it compatible with water-ice research, which is an important topic of lunar polar science. The upgraded PEACh can also work as a testbed for lunar mission payloads. We integrated a liquid-injection system to provide periodic water supply, upgraded the temperature control system to have both heating and cooling capabilities (the original PEACh had only cooling), added the energetic electron impact (EEI) accessories to simulate space weathering and to produce activated grain surfaces in a powdered sample, and a plasma probe to monitor the gas composition (to monitor the ions and free radicals as the breakdown products of various gases by EEI). Additionally, considering the aridity of the Moon, we developed a vacuum baking system to remove adsorbed water from terrestrial analog materials, thus eliminating an interference factor.

Here, we present the technical details of the whole facility, emphasize its performance tests, and demonstrate its potential applications through experiments on the hydration and dehydration of magnesium sulfate, which demonstrate the fundamental capabilities while showcasing the potential for investigating more complex issues such as lunar polar processes.

## 2. Technical description

### 2.1. The upgraded planetary environment and analysis chamber (PEACh)

The PEACh is a 24 × 24 × 24 inch stainless steel single-walled sealed chamber manufactured by the Kurt J. Lesker Company (Sobron and Wang, 2012). The PEACh was first built and tested in 2010-2012, with a core design including a rotating sample cell platter, controllable sample cooling ($LN_2$), an in-situ Raman probe, and a gas in & out with a pressure-monitoring subsystem. We upgraded the PEACh recently with new functionality, including a liquid injection system, a sample heating system coupled with the original cooling system, the energetic electron impact (EEI) accessories, a bluetooth-controlled camera, and an in-situ plasma spectral probe to monitor changes in gas composition. More details are shown in Figs. 1 and 2. The performance and the applications are described in sections 3 and 4.

#### 2.1.1. Environmental control

**Pressure**: The PEACh can maintain a pressure ranging from $7 \times 10^{-2}$ mbar to Earth atmospheric pressure using an oil-free scroll pump (Edwards XDS35i). Owing to chamber aging (in service for over 15 years), achieving $7 \times 10^{-2}$ mbar requires approximately 3 h, but it only takes 4 min to drop to 1 mbar. Though the pressure is not low enough to directly simulate conditions at the surface of airless bodies such as the Moon or Europa, we can fill the chamber with inert gas and displace the reactive gas ($N_2$, $O_2$, $CO_2$, $H_2O$, etc.) by multiple purges. After that, the chamber can simulate conditions in the shallow subsurface of such airless bodies. The effect of purging is monitored by plasma spectroscopy and presented in Section 3, Performance Tests. The pressure is measured using a PDR2000 Dual Capacitance Manometer (MKS Inc.), which is a versatile solution for all different gases.

**Gas composition**: The desired gas can be introduced into the PEACh through a needle valve. While the scroll pump runs, we can balance the gas inlet and outlet speed and maintain the desired pressure. The gas composition in the PEACh can be monitored by plasma spectroscopy using an in-situ probe, which is described in the next subsection: In-situ Analytical Methods.

**Temperature**: A hollow copper plate (refer to Figs. 1 and 2) is the core media in our temperature control system, and its temperature can be controlled between −100 °C and 100 °C. It has a channeled inner structure. The regulated $LN_2$ (liquid nitrogen) flows through the channels inside the copper plate when the system is in the cooling mode (more details shown in Fig. 4 of Sobron and Wang, 2012). Four heating pads adhered to the copper plate can heat the copper plate to 100 °C. The set value of temperature and the mode switch are controlled by an Omega Company CN8PT-144 Platinum series temperature controller. The sample cell carried by a rotating platter is in good thermal contact with the copper plate. Several thermocouples are used to monitor the temperatures in the PEACh, e.g., sample cell, copper plate, rotating platter, and PEACh wall (Fig. 5).

**Energetic Electron Impact (EEI)**: The EEI is generated by a pair of copper electrodes (35 mm in diameter) connected to a power source of tunable voltage from 0 to 40 kV. The sample cell (made of Teflon) is placed on the lower electrode, i.e., the sample is insulated from the copper electrode, but impacted by energetic electron flux between the two electrodes (photo in Fig. 8). In Fig. 1, the $V_1$ is an oscilloscope that measures the voltage between the two electrodes. $V_2$, combined with a parallel-connected resistor ($R = 4.7\ \Omega$), is equivalent to an ammeter that measures the total current between the two electrodes. An estimation of electron kinetic energy and flux density of the EEI can be calculated based on the measured voltage and current. The average electron kinetic energy is approximately $V_1$ (in unit eV). The electron flux density can be

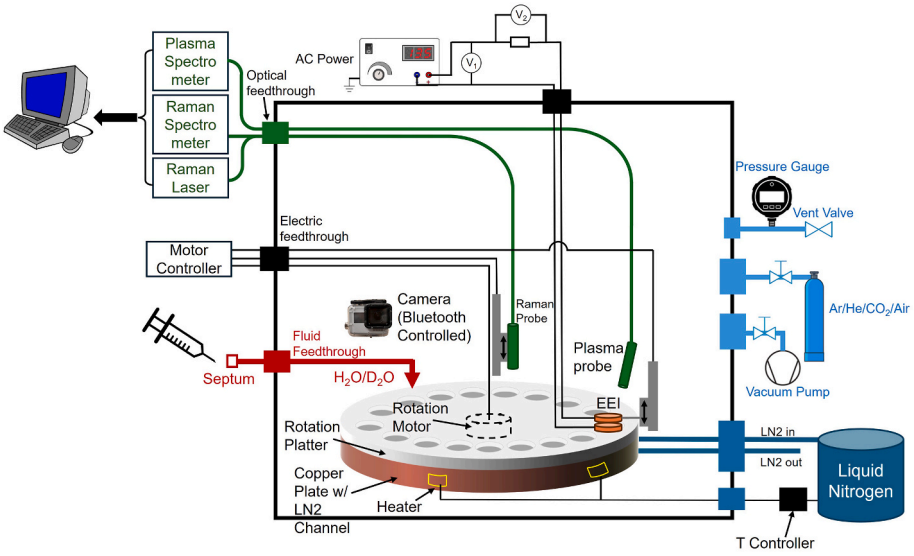


**Fig. 1.** Scheme of five subsystems in the upgraded PEACh.

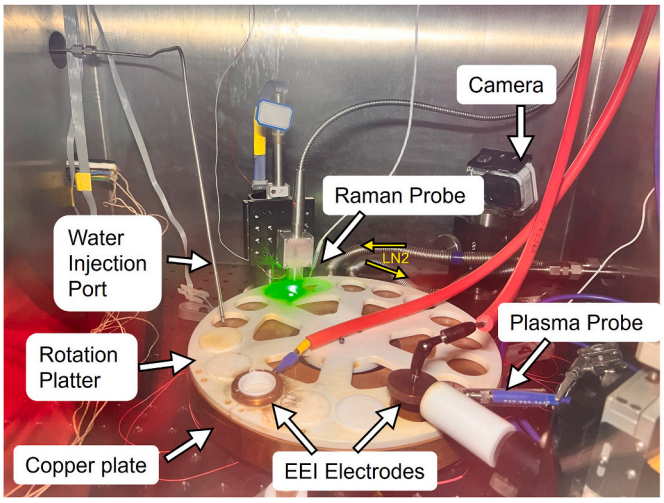


**Fig. 2.** Photo of the inside of the upgraded PEACh.

calculated by:

$$\text{Flux} = \frac{V_2}{R}\frac{1}{1.6\times10^{-19}}\frac{4}{\pi d^2}$$

Here, Flux is the electron flux density ($s^{-1}\cdot m^{-2}$), $V_2$ is the voltage (V) across the resistor measured by the #2 voltmeter, $R$ is the resistance (Ω), $d$ is the diameter (m) of the copper electrodes.

**Liquid injection system**: A stainless-steel tube (1/8" in diameter) with a septum sealing one end of the tube can introduce water ($D_2O$ or $H_2O$, in a syringe, Fig. 1) into the PEACh (across a feedthrough on the wall) and fill the sample cell while keeping the chamber pressure in the desired range. The syringe is manually operated; the precision is about ± 0.1 ml. Water will be drawn into the PEACh owing to the pressure difference inside and outside the chamber. To avoid immediate boiling or ice-beads forming (Steddum, 1971), the inner pressure of the PEACh should be higher than a certain value (e.g., we usually set the threshold to 60 mbar of Ar/He) when water is injected into the sample cell in the form of droplets.

### 2.1.2. *In-situ analytical methods*

The PEACh features two in-situ analytical methods: Raman spectroscopy for checking the status of the sample, and plasma spectroscopy for monitoring the gas composition.

**Raman spectroscopy**: The Raman spectroscopy system consists of a RamanRxn1 spectrograph (Kaiser Optical Systems, Inc.), 532 nm diode-pumped solid-state laser (Oxxius, Inc.), and a standalone Raman probe (InPhotonics, Inc.). Outside the PEACh, the Raman probe (6x1 configuration) is connected to the laser via a single-mode optical fiber and to the spectrograph via six multimode optical fibers (Fig. 1). At the output of the Raman probe inside the setup, the laser power is approximately 33 mW and is adjustable. The working distance of the Raman probe is about 5 mm, and its focus can be adjusted by a piezo stage motor (Thorlabs PD1V). An Andor DU401A-BV-132 iDus CCD camera is installed on the RamanRxn1 spectrograph to detect the Raman photons.

**Plasma spectroscopy**: The plasma spectroscopy system consists of three Ocean Optics HR2000+ spectrometers and an Ocean Optics custom probe with 4x1 optical fiber. Each HR2000+ spectrometer covers UV (238.594–339.268 nm), VIS (380.641–468.658 nm), and IR (459.589–910.794 nm) respectively. The spectral resolution of these spectrometers are 0.2 nm (Wu et al., 2018).

### 2.2. *Two-layer vacuum baking chamber for analog sample preparation*

The two-layer vacuum baking chamber consists of an inner tube furnace (Deltech, Inc.) inside a glove box (Plas Labs, Inc.). A sketch can be found in Fig. 3, with photos in Fig. 4. The tube furnace is evacuated by an Edwards E2M2 vacuum pump that can reach a pressure of 0.6 mbar.

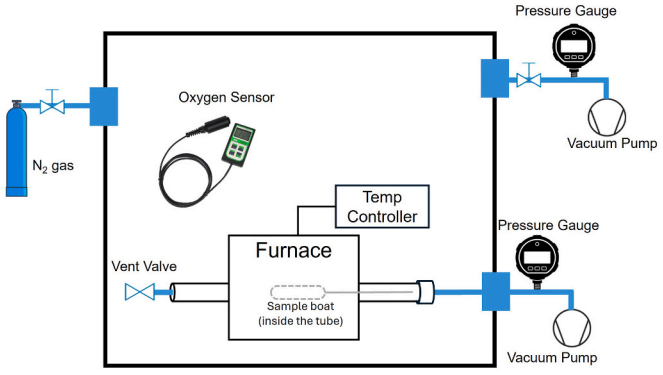


**Fig. 3.** Scheme of the two-layer system for vacuum baking for analog sample preparation.

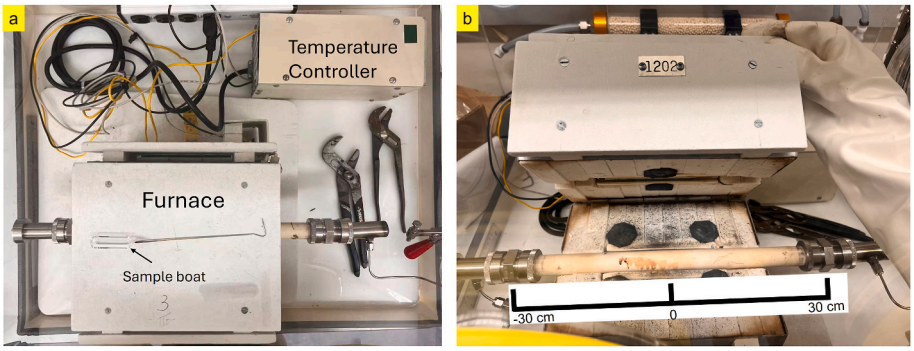


**Fig. 4.** Photos of the layout in the outer glove box (a) and the inner tube furnace (b) with a ruler to show the approximate scale. During the experiment, the sample boat in (a) is placed inside the tube in (b).

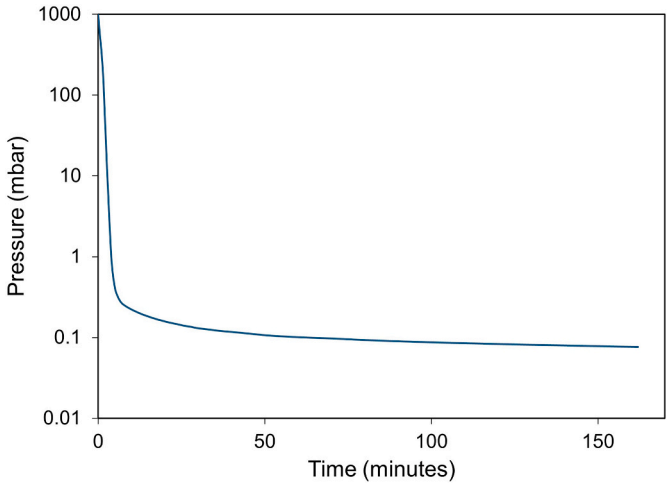


**Fig. 5.** The measured pressure in the PEACh during the establishment of a vacuum.

The temperature inside the tube furnace is controlled by a Fuji Electric PXF4 temperature controller. The controller sets the temperature to the desired value (Fig. 11). We usually set the center of the tube furnace to 500 °C to remove terrestrial $H_2O$ adsorbed on the surface of analog samples (powdered olivine and basaltic glass for a lunar analog study). An $N_2$ gas tank and a Welch 1400 DuoSeal vacuum pump are connected to the outer glove box so we can purge the glove box multiple times until the oxygen concentration reaches the lowest level (measured by an oxygen sensor, Apogee SO-130, uncertainty = ±1% of the measured oxygen concentration). This procedure minimizes oxidation during the short period of transferring the vacuum baked sample particles from the tube furnace to the PEACh.

As an example of this procedure, after the removal of a sample boat that contains sample particles (Fig. 3) from the inner tube furnace into the outer glove box that was filled with dry $N_2$ with extremely low $O_2$ (Fig. 12), the sample particles were immediately placed into a reaction sample cell (made of Teflon) filled with $D_2O$. This reaction cell was then immediately transferred into the PEACh, whose initial vacuum (1 mbar) could be reached in 4 min, and then continuously purged with inert Ar gas for 6 times to remove the reactive gases ($N_2$, $O_2$, $CO_2$, $H_2O$). This process effectively prevents the re-adsorption of terrestrial $H_2O$ and oxidation of analog samples.

## 3. Performance tests

### 3.1. PEACh vacuum test

The upgraded PEACh can now reach a minimum pressure of ~0.7 mbar. It reaches 0.0762 mbar after 160 min, only slightly poorer than the initial performance (0.018 mbar after 150 min, Table 2 in Sobron and Wang, 2012). The main cause of the difference in performance is the additional feedthroughs installed for the current version of the chamber. The septum in the water-injection system can also cause gas leaks.

### 3.2. PEACh temperature test

The copper plate can be heated to 100 °C in about 1 h. However, it takes time for heat to transfer to the sample cell. Thus, we measured the temperature using multiple thermocouples, on the copper plate, the Teflon rotation platter, and the lower electrode (in the order of heat transfer, refer to Fig. 2 for their relative position). The sample inside the Teflon cell on the lower electrode can reach ~65 °C after around 2 h (Fig. 6), while the temperatures on the copper plate and on the Teflon rotation platter both reach their maximum around 1 h. For water-rock

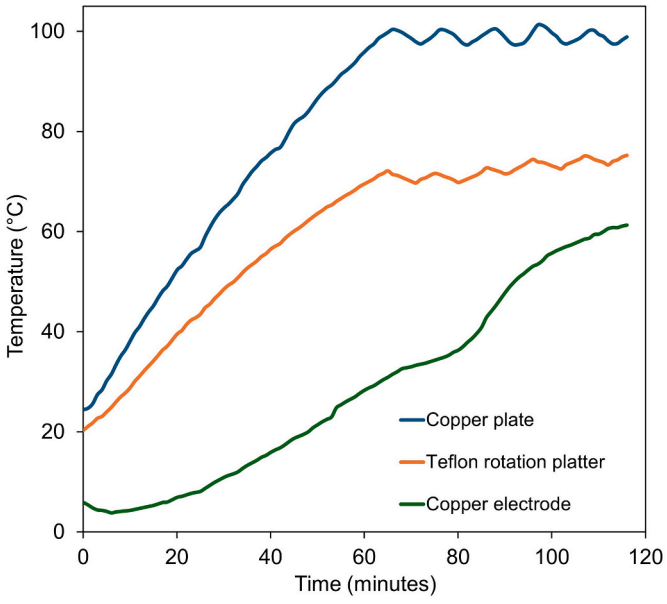


**Fig. 6.** Temperature profile of three different spots in PEACh (copper plate, Teflon rotation platter, and the lower copper electrode that carries the Teflon sample cell) as a function of time during the heating process. (Set point is 100 °C.)

reactions at this temperature, the pressure (inert gas Ar) should be kept >300 mbar to prevent water from boiling.

In cooling mode, the copper plate temperature drops to −100 °C in around 100 min. This is an effective simulation of the nighttime temperatures experienced in the equatorial regions of both the Moon and Mars.

### 3.3. PEACh EEI and plasma probe test

The EEI strength is determined by the gas composition and pressure. Higher pressure makes it more difficult to ionize the gas (Fig. 8), and a gas with lower mass (e.g., He) is easier to ionize. The plasma probe can acquire the emission spectra of the EEI glow, providing us with the ability to check the gas composition inside the chamber qualitatively (Figs. 9 and 10). Though it is difficult to repel water vapor out of the chamber completely, running the vacuum pump for a long time (a few days) and multiple purges (6 times, Fig. 10) with Argon gas can decrease the content of water vapor considerably inside the chamber (Fig. 10). A single purge cycle is defined as evacuating the chamber to <0.5 mbar, followed by filling with high-purity Ar gas to 1 bar. The decrease of water vapor concentration can be monitored by OH and Hα emission lines (Fig. 10).

### 3.4. Vacuum sample baking temperature profile and the effect of $N_2$ purging

The core component of the vacuum sample baking system – the tube furnace, can remove all adsorbed $H_2O$ or OH from mineral grain surfaces at a temperature of 500 °C in 4 h (Fukuda, 2012) as long as the sample boat is placed in the middle of the tube. The temperature drops as it is closer to each end of the tube (see Fig. 11).

A typical way to simulate water-rock interactions is to place the sample and water in a sealed container for a long duration, e.g., a pressurized reaction vessel or a sealed tube (Mayhew et al., 2013; Perronnet et al., 2007). We used repetitive purging (>10 times) with $N_2$ gas into the glove box to create a low-oxygen atmosphere (Fig. 12, as low as 1.7%, measured using an oxygen sensor) so that the sample (to-be-reacted in the PEACh) can be sealed in $D_2O$ under a low oxygen atmosphere. Our definition of one $N_2$ purge in the glove box is to use the vacuum pump to get the two gloves fully inflated inwards, then filling the glove box with nitrogen until the two gloves get fully inflated outwards.

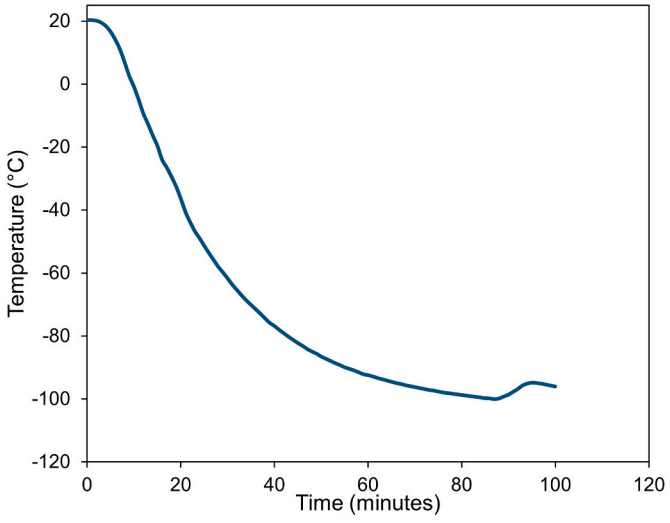


**Fig. 7.** Temperature profile of the copper plate as a function of time during the cooling process. (Set point −100 °C.)

## 4. Application: simulating aqueous alteration in the PEACh

The in-situ Raman probe in the PEACh can monitor the aqueous alteration of the samples. We select magnesium sulfate samples as an example because their dehydration and rehydration rates are rapid, and their changes in Raman spectroscopy are obvious and well-studied (A. Wang et al., 2009). For example, Magnesium sulfate could be hydrated to different hydration degrees, which can be revealed by the $\nu_1(SO_4)$ Raman peak position and the shape of structural water peaks (A. Wang et al., 2009). In-situ Raman characterization could also distinguish the effect of Earth atmosphere, such as oxygen, carbon dioxide, or water vapor. For example, if a sample for simulation study has already altered because of exposure to the Earth atmosphere (thus has $H_2O$ or OH in its structure or adsorbed at the grain surface), further simulation of water-solid reactions would be meaningless. For that purpose, we would use $D_2O$ instead of $H_2O$ for simulation reactions, since $D_2O$ has well-characterized Raman peaks (Fig. 13).

To demonstrate the upgraded PEACh application potential as a reaction chamber with in-situ sensing capability, we use kieserite ($MgSO_4{\cdot}H_2O$) and $H_2O$ water to demonstrate the PEACh's ability to simulate aqueous alteration and use epsomite ($MgSO_4{\cdot}7H_2O$) with EEI to demonstrate the effect of dehydration and amorphization by EEI. The experiments for simulating aqueous alteration on another planetary body (e.g., the Moon) will require greater reaction durations.

### 4.1. Hydration of kieserite in PEACh by water injection

Starting from 0.5 g kieserite ($MgSO_4{\cdot}H_2O$) in the Teflon reaction cell, we gradually added $H_2O$ water through the liquid injection port on the PEACh. Magnesium sulfate reacts quickly with water, then we use the Raman probe to examine the different hydration degrees (Fig. 14). By comparing the peak position and shapes reported in Wang et al. (2009), we can infer that adding 1 ml water to 0.5 g kieserite will convert it into $MgSO_4{\cdot}3H_2O$; adding another 1 ml (for a cumulative total of 2 ml) water to 0.5 g kieserite will convert it to hexahydrite ($MgSO_4{\cdot}6H_2O$); and adding another 2 ml (for a cumulative total of 4 ml) water is enough to saturate the sample and produce epsomite ($MgSO_4{\cdot}7H_2O$). This test also demonstrates the effectiveness of each related system (liquid injection port and Raman probe) and the workflow, which can be applied to more complex experiments on water-rock interactions.

### 4.2. Dehydration and amorphization of epsomite by EEI

We applied EEI to 1 g epsomite ($MgSO_4{\cdot}7H_2O$) in the Teflon cell and collected the Raman spectra of the sample every 5 min. The average electron energy is 275 eV, which falls within the natural 7 eV to 20 keV range of the lunar surface. The average flux density is about $1 \times 10^{19}$ $s^{-1}$ $m^{-2}$. This flux value is significantly higher than actual conditions to simulate long-term natural irradiation within just a few hours. Fig. 15 shows how the sample dehydrates as a function of EEI exposure time. It takes less than 5 min to dehydrate the sample into hexahydrite ($MgSO_4{\cdot}6H_2O$). After 20 min, a new peak occurs, but much wider, whose position (1021 $cm^{-1}$) is near that of $MgSO_4{\cdot}3H_2O$. Longer EEI exposure caused this peak to become stronger and wider (Fig. 15). The peak of crystalline Mg-sulfate totally disappeared after 30 min. After 60 and 120 min of EEI, the center of the broad peak matched the peak position of sanderite ($MgSO_4{\cdot}2H_2O$), (compared with A. Wang et al., 2009). This broad, strong peak is a clear sign that EEI causes the amorphization of the hydrous sulfate (Fig. 7 of A. Wang et al., 2009), which resembles space weathering to some extent.

The heating effect of EEI and the Raman laser cannot be the main reason for the dehydration and amorphization for the following reason: the heating effect of the Raman laser does not have a dehydration effect on magnesium sulfate in this case, because in the hydration experiment it eventually formed $MgSO_4{\cdot}7H_2O$. The thermogravimetric analysis (TGA) indicates that 65 °C (caused by EEI) only decomposes

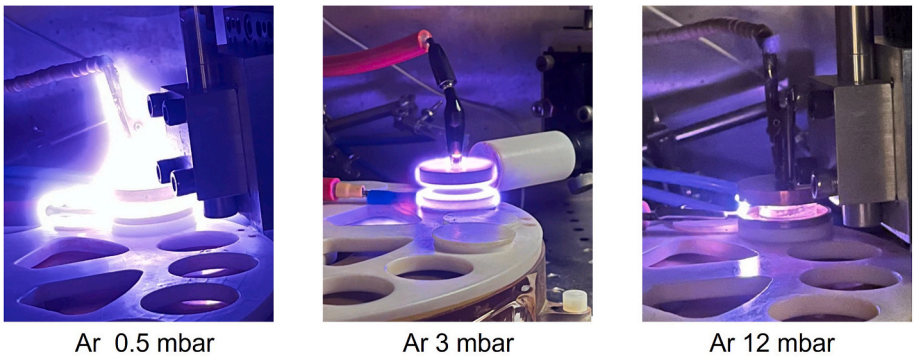


**Fig. 8.** Images of EEI in an argon atmosphere. The glow is best at around 3 mbar, which generates a homogeneous energetic electron impact (EEI) onto the analog sample inside the Teflon cell that is placed in the lower electrode.

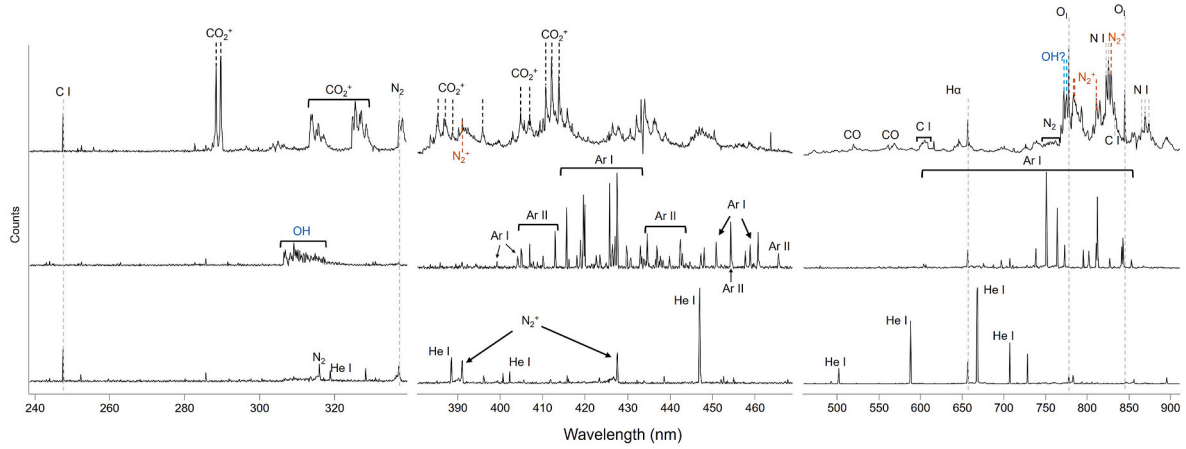


**Fig. 9.** The plasma spectra of EEI in the atmosphere in $CO_2$, Ar, and He (from top to bottom). The primary breakdown products are C, CO, $CO_2^+$ in $CO_2$; Ar I, and Ar II in Ar; He I and He II in He. Additional lines of $N_2$, $N_2^+$, N, O, OH, H are from residual atmospheric contamination.

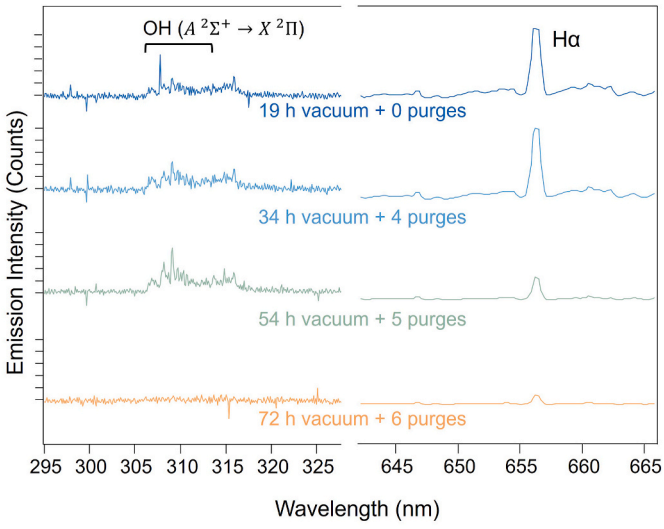


**Fig. 10.** Plasma spectra at the OH and Hα emission lines region. From top to bottom: increasing duration in vacuum pumping and more purges with Ar can reduce the intensities of OH and Hα line, i.e., enhancing the repelling effect of terrestrial $H_2O$.

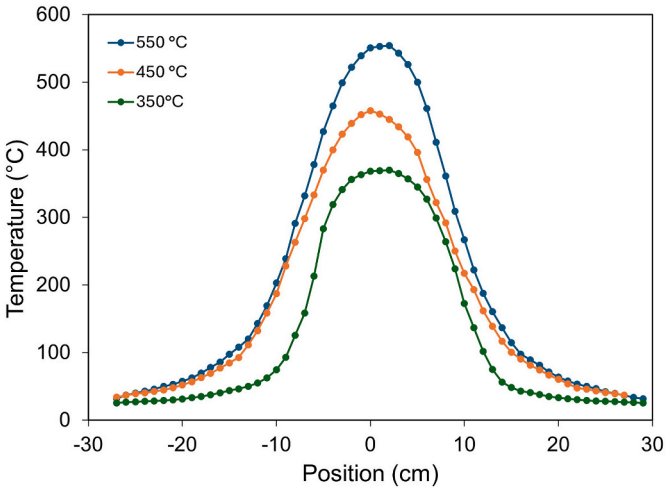


**Fig. 11.** Temperature distribution in the tube furnace. Credit: Qu et al. (2023).

$MgSO_4{\cdot}7H_2O$ into $MgSO_4{\cdot}6H_2O$, without further decomposition (Akcaoglu et al., 2020), i.e., the heating effect might contribute to the decomposition of $MgSO_4{\cdot}7H_2O$ into $MgSO_4{\cdot}6H_2O$, but it is unlikely to cause $MgSO_4{\cdot}6H_2O$ to decompose further into $MgSO_4{\cdot}2H_2O$.

## 5. Summary and future directions

The upgraded PEACh at Washington University in St. Louis can simulate planetary processes and chemical reactions with its EEI accessories, liquid injection system, pressure (0.7 mbar to 1020 mbar) and

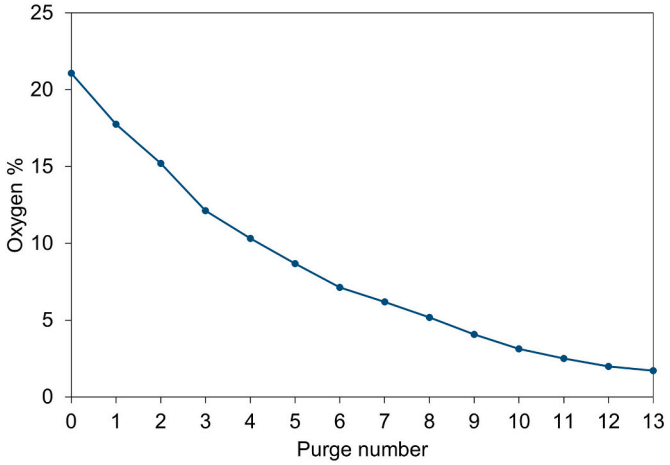


**Fig. 12.** Oxygen content in the glove box as a function of the number of purges (measured and calibrated using an oxygen sensor).

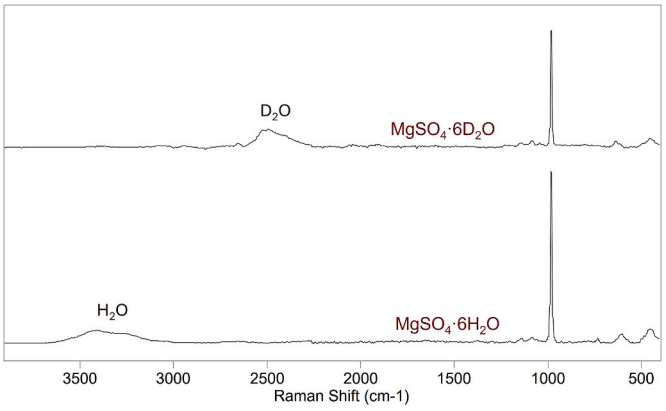


**Fig. 13.** Raman spectra of $D_2O$-bearing Mg-sulfate (top) and $H_2O$-bearing Mg-sulfate (bottom), measured using the in-situ Raman probe.

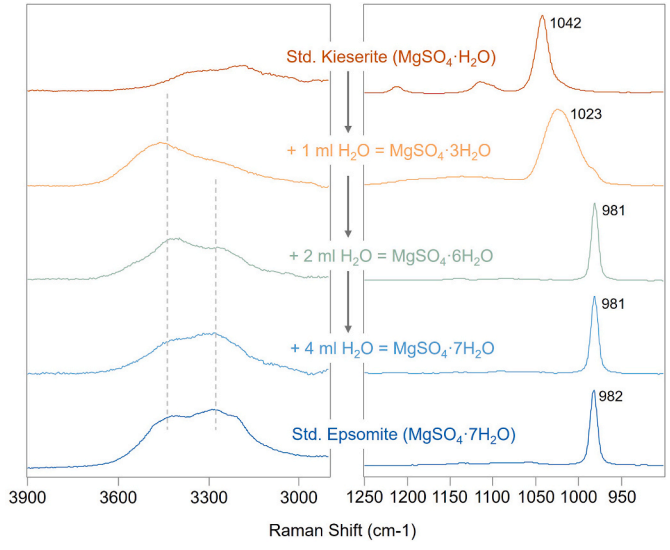


**Fig. 14.** Raman spectra of starting kieserite (top), the products after kieserite reacts with different volumes of injected water, and standard epsomite for reference (bottom).

temperature (−100 to 100 °C) control. It not only can simulate an atmospheric condition by introducing the specific gas into the chamber, but it can also simulate an airless body by multiple purges with an inert gas (e.g., argon). Hence, from the perspective of chemical reactions, it maintains the partial pressure of reactive gases ($N_2$, $O_2$, $CO_2$, $H_2O$, etc.) much lower than its lower limit (0.7 mbar), so that the reactants are well-constrained. The PEACh also has several in-situ sensors and probes, including a Raman probe to measure the Raman spectra of the reactants and products, a plasma probe to monitor the gas composition in the environment, and a bluetooth camera to view the sample. It provides the ability to minimize effects of the Earth's atmosphere and temperature that might cause chemical changes to the samples by in-situ measurement.

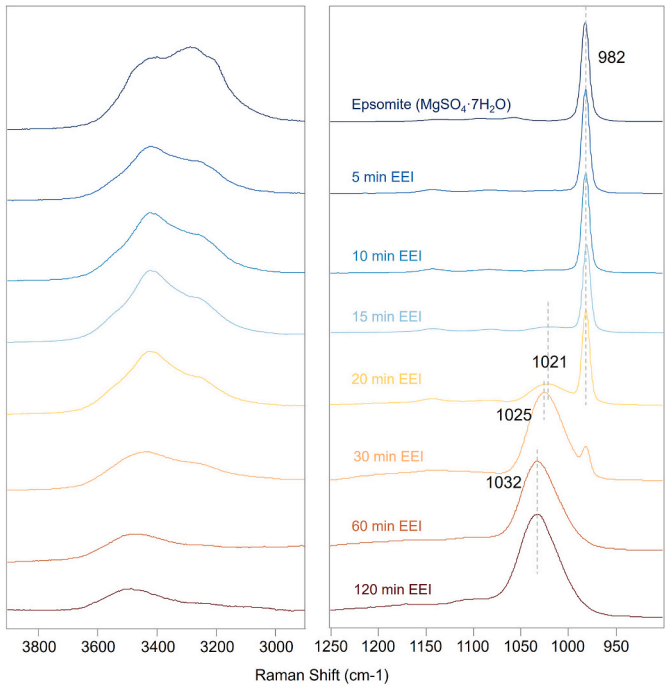


**Fig. 15.** Raman spectra of starting epsomite (top) and the products after different durations of EEI irradiation (from top to bottom, 5 min to 120 min).

Plans for future applications of the upgraded PEACh include the following: We are designing a series of hydration experiments with EEI as a simulation of space weathering to study the water-regolith interactions in the polar regions of the Moon. Importantly, hydrated minerals are crucial signatures to understanding the history of a planetary body's water activity. A similar logic can be easily applied to Mars or Pluto, whose atmospheric pressure in the range of the PEACh. The lower temperature limit of the PEACh could be extended far below −100 °C by circulating liquid helium instead of liquid nitrogen in the channels inside the copper plate. Thus, the PEACh could simulate the environment of icy moons in our Solar System, which have drawn more interest recently because of the discovery of massive storage of water, and the potential bond between water and astrobiology.

## CRediT authorship contribution statement

**Chengzheng Yong:** Data curation, Investigation, Writing – original draft, Writing – review & editing. **Alian Wang:** Conceptualization, Writing – review & editing. **Chuck Y.C. Yan:** Methodology. **Bradley L. Jolliff:** Funding acquisition, Writing – review & editing.

## Declaration of competing interest

The authors declare that they have no known competing financial interests or personal relationships that could have appeared to influence

the work reported in this paper.

## Acknowledgements

This work is supported by the SSERVI node ICE Five-O (Interdisciplinary Consortium for Evaluating Volatile Origins, NNA80NSSC20M0027), the PI, Jeff Gillis, and the McDonnell Center for the Space Sciences at Washington University in St. Louis.

## Data availability

Data will be made available on request.

## References

Akcaoglu, S.C., Sun, Z., Moratti, S.C., Martinopoulos, G., 2020. Investigation of novel composite materials for thermochemical heat storage systems. Energies 13 (5), 1042. https://doi.org/10.3390/en13051042.

Beegle, L., Bhartia, R., White, M., DeFlores, L., Abbey, W., Wu, Yen-Hung, Cameron, B., Moore, J., Fries, M., Burton, A., Edgett, K.S., Ravine, M.A., Hug, W., Reid, R., Nelson, T., Clegg, S., Wiens, R., Asher, S., Sobron, P., 2015. SHERLOC: scanning habitable environments with Raman & luminescence for organics & chemicals. 2015 IEEE Aerospace Conference 1–11. https://doi.org/10.1109/AERO.2015.7119105.

Buffo, C.E., Jones, B.M., Orlando, T.M., 2025. Water ice formed by vapor deposition and liquid aerosol injection: a comparison study using reflectance absorption infrared spectroscopy. J. Chem. Phys. 162 (24), 244509. https://doi.org/10.1063/5.0261149.

Campbell, B.A., 2016. Planetary geology with imaging radar: insights from earth-based lunar studies, 2001–2015. Publ. Astron. Soc. Pac. 128 (964), 062001. https://doi.org/10.1088/1538-3873/128/964/062001.

Cho, Y., Böttger, U., Rull, F., Hübers, H.-W., Belenguer, T., Börner, A., Buder, M., Bunduki, Y., Dietz, E., Hagelschuer, T., Kameda, S., Kopp, E., Lieder, M., Lopez-Reyes, G., Moral Inza, A.G., Mori, S., Ogura, J.A., Paproth, C., Perez Canora, C., et al., 2021. In situ science on Phobos with the Raman spectrometer for MMX (RAX): preliminary design and feasibility of Raman measurements. Earth Planets Space 73 (1), 232. https://doi.org/10.1186/s40623-021-01496-z.

Clark, R.N., 2009. Detection of Adsorbed water and hydroxyl on the Moon. Science 326 (5952), 562–564. https://doi.org/10.1126/science.1178105.

Colaprete, A., Andrews, D., Bluethmann, W., Elphic, R.C., Bussey, B., Trimble, J., Zacny, K., Captain, J.E., 2019. An overview of the volatiles investigating polar Exploration rover (VIPER) mission. AGU Fall Meeting Abstracts, 2019, P34B-03.

Colaprete, A., Schultz, P., Heldmann, J., Wooden, D., Shirley, M., Ennico, K., Hermalyn, B., Marshall, W., Ricco, A., Elphic, R.C., Goldstein, D., Summy, D., Bart, G.D., Asphaug, E., Korycansky, D., Landis, D., Sollitt, L., 2010. Detection of water in the LCROSS ejecta plume. Science 330 (6003), 463–468. https://doi.org/10.1126/science.1186986.

Craig, M., Cloutis, E.A., Mueller, T., 2001. ME and Mini-ME: two Mars environmental simulation chambers for reflectance spectroscopy. 42nd Lunar and Planetary Science Conference 1368. https://ui.adsabs.harvard.edu/abs/2001LPI ....32.1368C.

Donaldson Hanna, K.L., Bowles, N.E., Warren, T.J., Hamilton, V.E., Schrader, D.L., McCoy, T.J., Temple, J., Clack, A., Calcutt, S., Lauretta, D.S., 2021. Spectral characterization of bennu analogs using PASCALE: a new experimental set-up for simulating the near-surface conditions of airless bodies. J. Geophys. Res. Planets 126 (2). https://doi.org/10.1029/2020JE006624 e2020JE006624.

Feldman, W.C., Lawrence, D.J., Elphic, R.C., Barraclough, B.L., Maurice, S., Genetay, I., Binder, A.B., 2000. Polar hydrogen deposits on the Moon. J. Geophys. Res. Planets 105 (E2), 4175–4195. https://doi.org/10.1029/1999JE001129.

Feldman, W.C., Maurice, S., Binder, A.B., Barraclough, B.L., Elphic, R.C., Lawrence, D.J., 1998. Fluxes of fast and epithermal neutrons from lunar prospector: evidence for water ice at the lunar poles. Science 281 (5382), 1496–1500. https://doi.org/10.1126/science.281.5382.1496.

Fukuda, J., 2012. Water in rocks and minerals—species, distributions, and temperature dependences. In: Theophanides, T. (Ed.), Infrared Spectroscopy—Materials Science, Engineering and Technology. InTech. https://doi.org/10.5772/35668.

Gillis, J.J., 2022. The ability to laser space weather in multiple microenvironments. 53rd Lunar and Planetary Science Conference 2678 (2465). LPI Contribution. https://ui.adsabs.harvard.edu/abs/2022LPICo2678.2465G/abstract.

Herczku, P., Mifsud, D.V., Ioppolo, S., Juhász, Z., Kaňuchová, Z., Kovács, S.T.S., Traspas Muiña, A., Hailey, P.A., Rajta, I., Vajda, I., Mason, N.J., McCullough, R.W., Paripás, B., Sulik, B., 2021. The ice Chamber for astrophysics–Astrochemistry (ICA): a new experimental facility for ion impact studies of astrophysical ice analogs. Rev. Sci. Instrum. 92 (8), 084501. https://doi.org/10.1063/5.0050930.

Herny, C., Conway, S.J., Raack, J., Carpy, S., Colleu-Banse, T., Patel, M.R., 2019. Downslope sediment transport by boiling liquid water under Mars-like conditions: experiments and potential implications for Martian gullies. Geological Society 467 (1), 373–410. https://doi.org/10.1144/SP467.10. London, Special Publications.

Mateo-Martí, E., Prieto-Ballesteros, O., Sobrado, J.M., Gómez-Elvira, J., Martín-Gago, J. A., 2006. A chamber for studying planetary environments and its applications to astrobiology. Meas. Sci. Technol. 17 (8), 2274–2280. https://doi.org/10.1088/0957-0233/17/8/031.

Mattioda, A.L., Gavilan, L., Ricketts, C.L., Najeeb, P.K., Ricca, A., Boersma, C., 2024. The NASA Raman spectroscopic database: ramdb version 1.00. Icarus 408, 115769. https://doi.org/10.1016/j.icarus.2023.115769.

Maurice, S., Wiens, R.C., Bernardi, P., Caïs, P., Robinson, S., Nelson, T., Gasnault, O., Reess, J.-M., Deleuze, M., Rull, F., Manrique, J.-A., Abbaki, S., Anderson, R.B., André, Y., Angel, S.M., Arana, G., Battault, T., Beck, P., Benzerara, K., et al., 2021. The SuperCam instrument suite on the Mars 2020 rover: science objectives and mast-unit description. Space Sci. Rev. 217 (3), 47. https://doi.org/10.1007/s11214-021-00807-w.

Mayhew, L.E., Ellison, E.T., McCollom, T.M., Trainor, T.P., Templeton, A.S., 2013. Hydrogen generation from low-temperature water–rock reactions. Nat. Geosci. 6 (6), 478–484. https://doi.org/10.1038/ngeo1825.

Palumbo, M.E., Ferini, G., Baratta, G.A., 2004. Infrared and Raman spectroscopies of refractory residues left over after ion irradiation of nitrogen-bearing icy mixtures. Adv. Space Res. 33 (1), 49–56. https://doi.org/10.1016/j.asr.2003.03.002.

Perronnet, M., Berger, G., Zolensky, M.E., Toplis, M.J., Kolb, V.M., Bajagic, M., 2007. The aqueous alteration of CR chondrites: experiments and geochemical modeling. 38th Lunar and Planetary Science Conference 1110. https://ntrs.nasa.gov/api/citations/20070011758/downloads/20070011758.pdf.

Pieters, C.M., Goswami, J.N., Clark, R.N., Annadurai, M., Boardman, J., Buratti, B., Combe, J.-P., Dyar, M.D., Green, R., Head, J.W., Hibbitts, C., Hicks, M., Isaacson, P., Klima, R., Kramer, G., Kumar, S., Livo, E., Lundeen, S., Malaret, E., et al., 2009. Character and spatial distribution of OH/H $_2$ O on the surface of the Moon seen by M $^3$ on Chandrayaan-1. Science 326 (5952), 568–572. https://doi.org/10.1126/science.1178658.

Qu, H.K., Wang, A., Thimsen, E., Ling, Z.C., 2023. Simulation of Venus lightning-I: characterization of free radicals generated in Venus major gas mixture. J. Geophys. Res. Planets 128 (5). https://doi.org/10.1029/2022JE007617 e2022JE007617.

Rabbow, E., Parpart, A., Reitz, G., 2016. The planetary and space simulation facilities at DLR cologne. Microgravity Sci. Technol. 28 (3), 215–229. https://doi.org/10.1007/s12217-015-9448-7.

Sanin, A.B., Mitrofanov, I.G., Litvak, M.L., Malakhov, A., Boynton, W.V., Chin, G., Droege, G., Evans, L.G., Garvin, J., Golovin, D.V., Harshman, K., McClanahan, T.P., Mokrousov, M.I., Mazarico, E., Milikh, G., Neumann, G., Sagdeev, R., Smith, D.E., Starr, R.D., Zuber, M.T., 2012. Testing lunar permanently shadowed regions for water ice: LEND results from LRO. J. Geophys. Res. Planets 117 (E12). https://doi.org/10.1029/2011JE003971, 2011JE003971.

General survey of vibrational spectroscopy. In: Schrader, B. (Ed.), 1995. Infrared and Raman Spectroscopy, first ed. Wiley, pp. 7–61. https://doi.org/10.1002/9783527615438.ch02.

Sears, D.W.G., Benoit, P.H., McKeever, S.W.S., Banerjee, D., Kral, T., Stites, W., Roe, L., Jansma, P., Mattioli, G., 2002. Investigation of biological, chemical and physical processes on and in planetary surfaces by laboratory simulation. Planet. Space Sci. 50 (9), 821–828. https://doi.org/10.1016/S0032-0633(02)00056-9.

Sobron, P., Wang, A., 2012. A planetary environment and analysis chamber (PEACh) for coordinated Raman-LIBS-IR measurements under planetary surface environmental conditions: planetary environmental chamber for coordinated Raman-LIBS-IR measurements. J. Raman Spectrosc. 43 (2), 212–227. https://doi.org/10.1002/jrs.3017.

Steddum, R.E., 1971. Characteristics Of Water Sprays Under Vacuum Conditions [Ph.D., Louisiana State University and Agricultural & Mechanical College]. In: Proquest Dissertations and Theses. ProQuest Dissertations & Theses Global, 302626999. https://www.proquest.com/docview/302626999/fulltextPDF/9D1639B459BB451DPQ/1?accountid=15159&sourcetype=Dissertations%20&%20Theses.

Stopar, J.D., Jolliff, B.L., Speyerer, E.J., Asphaug, E.I., Robinson, M.S., 2018. Potential impact-induced water-solid reactions on the Moon. Planet. Space Sci. 162, 157–169. https://doi.org/10.1016/j.pss.2017.05.010.

Sunshine, J.M., Farnham, T.L., Feaga, L.M., Groussin, O., Merlin, F., Milliken, R.E., A'Hearn, M.F., 2009. Temporal and spatial variability of lunar hydration as observed by the deep impact spacecraft. Science 326 (5952), 565–568. https://doi.org/10.1126/science.1179788.

Suttle, M.D., King, A.J., Ramkissoon, N.K., Bonato, E., Franchi, I.A., Malley, J., Schofield, P.F., Najorka, J., Salge, T., Russell, S.S., 2022. Alteration conditions on the CM and CV parent bodies – insights from hydrothermal experiments with the CO chondrite kainsaz. Geochem. Cosmochim. Acta 318, 83–111. https://doi.org/10.1016/j.gca.2021.11.028.

Vakkada Ramachandran, A., Nazarious, M.I., Mathanlal, T., Zorzano, M.-P., Martín-Torres, J., 2020. Space environmental chamber for planetary studies. Sensors 20 (14), 3996. https://doi.org/10.3390/s20143996.

Veneranda, M., Lopez-Reyes, G., Manrique-Martinez, J.A., Sanz-Arranz, A., Lalla, E., Konstantinidis, M., Moral, A., Medina, J., Rull, F., 2020. ExoMars Raman Laser Spectrometer (RLS): development of chemometric tools to classify ultramafic igneous rocks on Mars. Sci. Rep. 10 (1), 16954. https://doi.org/10.1038/s41598-020-73846-y.

Wang, A., Freeman, J.J., Jolliff, B.L., 2009. Phase transition pathways of the hydrates of magnesium sulfate in the temperature range 50°C to 5°C: implication for sulfates on Mars. J. Geophys. Res. 114 (E4), E04010. https://doi.org/10.1029/2008JE003266.

Wang, A., Haskin, L.A., Cortez, E., 1998. Prototype raman spectroscopic sensor for *in Situ* mineral characterization on planetary surfaces. Appl. Spectrosc. 52 (4), 477–487. https://doi.org/10.1366/0003702981943842.

Wang, A., Jolliff, B.L., Haskin, L.A., 1995. Raman spectroscopy as a method for mineral identification on lunar robotic exploration missions. J. Geophys. Res. 100 (E10), 21189. https://doi.org/10.1029/95JE02133.

Wang, C., Jia, Y., Xue, C., Lin, Y., Liu, J., Fu, X., Xu, L., Huang, Y., Zhao, Y., Xu, Y., Gao, R., Wei, Y., Tang, Y., Yu, D., Zou, Y., 2024. Scientific objectives and payload

configuration of the Chang'E-7 mission. Natl. Sci. Rev. 11 (2). https://doi.org/10.1093/nsr/nwad329 nwad329.

Weber, I., Böttger, U., Hanke, F., Reitze, M.P., Heeger, M., Adolphs, T., Arlinghaus, H.F., 2022. Space weathering simulation of micrometeorite bombardment on silicates and their mixture for space application. J. Raman Spectrosc. 53 (3), 411–419. https://doi.org/10.1002/jrs.6162.

Weber, I., Pavlov, S.G., Böttger, U., Reitze, M.P., 2024. Alteration in the Raman spectra of characteristic rock-forming silicate mixtures due to micrometeorite bombardment. J. Raman Spectrosc. 55 (8), 901–913. https://doi.org/10.1002/jrs.6676.

Weber, R.C., Lawrence, S.J., Cohen, B.A., Bleacher, J.E., Boyce, J.W., Collier, M.R., Draper, D., Fagan, A.L., Fassett, C.I., Gaddis, L., Gross, J., Gruener, J.E., Heldmann, J.L., McCubbin, F.M., Mitchell, J.L., Nahm, A.L., Needham, D.H., Noble, S., Pieters, C.M., et al., 2021. The Artemis III Science Definition Team Report, vol 1261. https://ui.adsabs.harvard.edu/abs/2021LPI ….52.1261W.

Wu, Z., Ling, Z., Zhang, J., Fu, X., Liu, C., Xin, Y., Li, B., Qiao, L., 2021. A Mars environment chamber coupled with multiple in situ spectral sensors for Mars exploration. Sensors 21 (7), 2519. https://doi.org/10.3390/s21072519.

Wu, Z., Wang, A., Farrell, W.M., Yan, Y., Wang, K., Houghton, J., Jackson, A.W., 2018. Forming perchlorates on Mars through plasma chemistry during dust events. Earth Planet Sci. Lett. 504, 94–105. https://doi.org/10.1016/j.epsl.2018.08.040.